This is a post-peer-review, pre-copyedit version of an article published in ***Microchimica Acta*** 188(4) : (2021) // Article ID 143. The final authenticated version is available online at: https://doi.org/10.1007/s00604-021-04804-2

Authors
Roberta Lanfranco, Janire Saez, Deborah Abati, Thomas Carzaniga, Fernando Benito-Lopez, Marco Buscaglia

Title
A microfluidic column of water index-matched packed microspheres for label-free observation of water pollutants

Affiliations
Roberta Lanfranco, Deborah Abati, Thomas Carzaniga, Marco Buscaglia: Department of Medical Biotechnology and Translational Medicine, University of Milan, via F.lli Cervi 93, 20054, Segrate (MI), Italy
Janire Saez, Fernando Benito-Lopez: Microfluidics Cluster UPV/EHU, Analytical Microsystems & Materials for Lab-on-a-Chip (AMMa-LOAC) Group, Analytical Chemistry Department, University of the Basque Country UPV/EHU, Barrio Sarriena s/n 48940 Leioa, Spain
Corresponding authors
Marco Buscaglia: marco.buscaglia@unimi.it (M. Buscaglia, via F.lli Cervi 93, 20090 Segrate, Italy)
Fernando Benito-Lopez: fernando.benito@ehu.eus (F. Benito-Lopez, Paseo de la Universidad, 7, 01006, Vitoria-Gasteiz, Spain)

ORCID
Roberta Lanfranco: 0000-0002-7240-8625
Janire Saez: 0000-0002-9246-0818
Thomas Carzaniga: 0000-0002-4236-4019
Fernando Benito-Lopez: 0000-0003-0699-5507
Marco Buscaglia: 0000-0001-5010-0278

Declarations
Funding: European Union's Seventh Framework Programme (FP7) for Research, Technological Development and Demonstration through the NAPES project, grant agreement no. 604241
Conflicts of interest/Competing interests: nothing to declare
Availability of data and material: the data that support the findings of this study are available from the corresponding authors, upon reasonable request.
Code availability: not applicable

Authors' contributions
Roberta Lanfranco: Conceptualization, Methodology, Formal analysis and investigation, Writing- Reviewing and Editing; Janire Saez: Methodology, Writing- Reviewing and Editing; Deborah Abati: Formal analysis and investigation, Visualization; Thomas Carzaniga: Data curation, Formal analysis and investigation, Visualization; Fernando Benito-Lopez: Supervision, Conceptualization, Resources, Writing- Reviewing and Editing; Marco Buscaglia: Supervision, Conceptualization, Resources, Writing- Original draft preparation.

Acknowledgments
We thank Emanuele Di Nicolò and Mattia Bassi for useful discussions. This research was funded by the European Union's Seventh Framework Programme (FP7) for Research, Technological Development and Demonstration through the NAPES project, grant agreement no. 604241.

A microfluidic column of water index-matched packed microspheres for label-free observation of water pollutants

Roberta Lanfranco [a], Janire Saez [b], Deborah Abati [a], Thomas Carzaniga [a], Fernando Benito-Lopez [b,*], Marco Buscaglia [a,*]

[a] Department of Medical Biotechnology and Translational Medicine, University of Milan, via F.lli Cervi 93, 20054, Segrate (MI), Italy
[b] Microfluidics Cluster UPV/EHU, Analytical Microsystems & Materials for Lab-on-a-Chip (AMMa-LOAC) Group, Analytical Chemistry Department, University of the Basque Country UPV/EHU, Barrio Sarriena s/n 48940 Leioa, Spain [*] Corresponding authors: marco.buscaglia@unimi.it (M. Buscaglia, via F.lli Cervi 93, 20090 Segrate, Italy), fernando.benito@ehu.eus (F. Benito-Lopez, Paseo de la Universidad, 7, 01006, Vitoria-Gasteiz, Spain)

Abstract

A microfluidic, label-free optical sensor for water pollutants, which is based on a packed micro-column of microspheres with refractive index similar to that of water, is presented. The perfluoropolyether microspheres are synthetized by membrane emulsification followed using UV irradiation. The microfluidic channel hosting the packed column is transparent when filled with pure water as a consequence of refractive index matching, whereas it scatters light in presence of compounds with lipophilic moieties that spontaneously adsorb on the fluorinated microspheres. The device is characterized by analysing the response to cationic and anionic surfactants. Both, the signal growth rate and the recovery rate measured during washing with water, depend on the type and concentration of the compounds. The cationic surfactant displays a larger signal increase, linearly scaling with concentration. A limit of detection of 6 μM is obtained in the current configuration. The water index-matched microspheres enable to access an additional analytical parameter, still largely unexplored, that is the propagation velocity of the scattering signal along the column. This parameter is also found to scale linearly with concentration, hence providing a complementary analytical tool sensitive to the adhesion kinetics.

Keywords: microfluidic device; label-free optical sensor; reflective phantom interface; scattering phantom interface; water index-matched materials; environmental monitoring.

Introduction

Water pollution is a constant concern worldwide being oils and surfactants especially harmful for human health and the environment. Therefore, they should be continually monitored to avoid spread of contamination [1]. Traditional methods to assess these pollutants require several analytical steps and largely use liquid chromatography techniques as gold standards in centralized laboratories, being not suitable for on-site monitoring [2]. In this sense, miniaturized liquid chromatography in microfluidics has been proven to provide rapid separations with smaller consumption of sample and reagents, being suitable for integration into remote, autonomous analytical platforms for the monitoring of water pollutants [3]. Miniaturized separation devices have been proposed in the form of either lateral flow membrane systems [4] or packed column of microspheres [5][6], with applications in cell capture and analysis [7][8], antibody separation [9], and nucleic acids detection [10][11]. Another potential advantage is the visualization of analytes binding/unbinding within the porous medium by optical imaging techniques, which have been shown to provide a more detailed understanding of the binding process [12]. Similarly, affinity and kinetics of microRNA hybridization targets confined in a nanofluidic channel have been measured from the analysis of time-resolved binding profiles on a long biosensor surface [13]. However, in both examples, the signal was provided by fluorescence, hence increasing the complexity of preparation and limiting the applicability of the methods. In contrast, label-free detection methods do not require

any labelling of the analytes and can be virtually applied to any class of target molecules. Nevertheless, the surface structure of a packed column of microspheres is not compatible with most optical label-free approaches, which typically require an extended planar surface, patterned with regular micro- or nano-structures [14]. A particularly simple and flexible approach is represented by the Reflective Phantom Interface (RPI) optical detection method [15][16], in which the signal arises from the formation of a thin molecular layer of analytes on a planar interface with very low reflectivity. The RPI method has been previously exploited to capture molecular targets by immobilized ligands [17][18][19][20], as well as to characterize the adsorption strength and kinetics on the surface of a prism of perfluorinated material that matches water's refractive index [21]. An analogous strategy, named as Scattering Phantom Interface (SPI) method [14][21][22], can be exploited to measure the amount of molecules binding on the internal surface of a micro-porous medium with refractive index similar to that of the liquid phase. In this approach, originated from a fundamental principle of optics, a collection of molecules freely diffusing in solution provide a very small light scattering, whereas the same amount of molecules confined in a shell with nm-scale thickness but extending on the micron scale yields to a much larger scattering contribution [23].
In this work, we present the design, characterization, and performance of a miniaturized device, composed by a packed column of water index-matched (WIM) micro-spheres hosted in a microfluidic channel, which enables the label-free optical measurement of molecular binding of surfactants by SPI. The device provides access to real-time binding profiles along the column without the need of labelling the analytes, and offers a larger set of characterization parameters, through the visualization of the analyte binding in flow, within the column.

2. Materials and Methods

2.1 Perfluoropolymers microspheres production

The WIM micro-spheres were produced by photo-polymerization of a micro-emulsion containing a dispersed phase composed by a mixture of 70 % (w/v) Fomblin MD40® and 30 % (w/v) Fomblin MD700® (Solvay Specialty Polymers, Italy, www.solvay.com), and a continuous phase of 4 % (w/v) sodium dodecyl sulphate (SDS) (Sigma-Aldrich, USA, www.sigmaaldrich.com) solution in water. Details on the selection of materials are provided as Electronic Supporting Material (ESM), section S1. (The fluorinated oils contained 0.1 % (w/v) Ciba Irgacure 651® (Ciba Specialty Chemicals, Switzerland) as photoinitiator to start the polymerization reaction. The micro-emulsion was prepared by the two-syringe emulsification method using membranes with 20 and 50 μm diameter pores (SPG Technology, Japan, www.spg-techno.co.jp). The emulsion was obtained after 20 times back and forth pushing between the two syringes, and then it was irradiated for 10 min with a 500 W UV lamp (Helios Italquartz, Italy, www.heliosquartz.com) under gentle agitation to avoid the aggregation of the microspheres. After polymerization, the fraction of largest microspheres or aggregates were discarded through sedimentation. The microspheres stability was tested through cycles of drying/wetting with ethanol and water before the insertion into the microfluidic device. Microspheres samples maintained their shape and size after repeated cycles, as well as after long-term storage. The size of the microspheres was measured by analyzing optical microscopy images through ImageJ (Figure 1a-b).

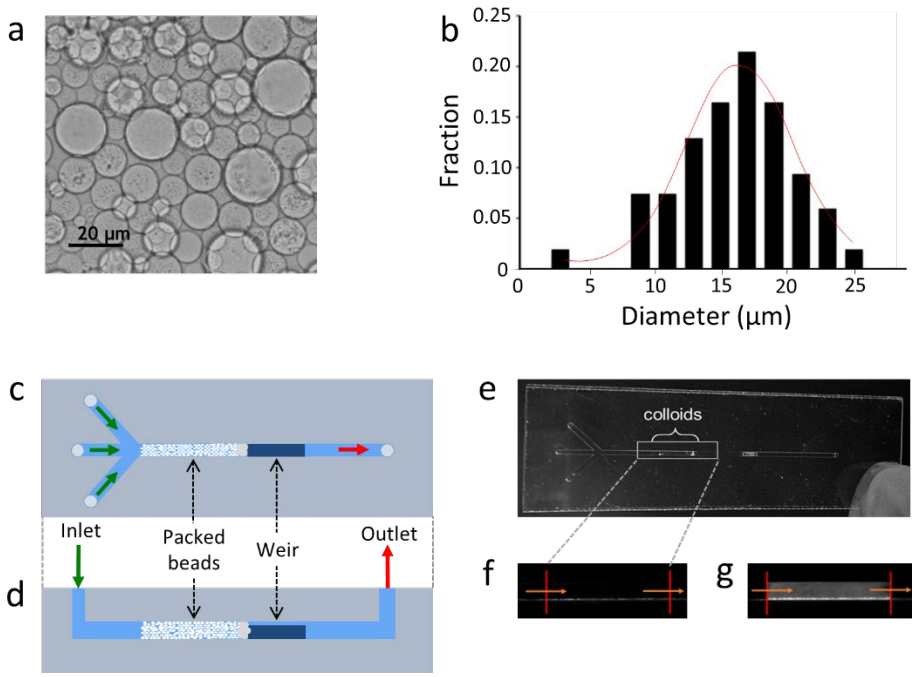

Figure 1. Scheme and pictures of the microfluidic device hosting the phantom microspheres. (a) Microscope image of the microspheres. (b) Size distribution of the microspheres. (c) Top view of the microfluidic device hosting the packed column. (d) Side section scheme of the microfluidic device. (e) Image of the fabricated device. Enlarged view of the part hosting the microspheres soaked with (f) deionized water (n_s = 1.333) and with (g) a NaCl 750 mM water solution (n_s = 1.340).

2.2 Microfluidic device fabrication

The microfluidic device was fabricated using a multilayer technique, as described in a previous work [24]. Briefly, five 100 µm layers of cyclo olefin polymer (COP, Zeonor COP sheets purchased from Zeonex, Germany), were xurographied by a FC8000-60 cutting plotter (Graphtec®, USA) and bonded by thermocompression [25]. The device was designed with three inlets (to prevent blocking of the channel with the microspheres) that converge in a 1 mm width channel, 300 µm height, which thinners to 100 µm close to the outlet (Figure 1c-d). The height reduction of the channel enabled to form a weir to pack the microspheres. A small amount of Hyflon AD® powder, which combines an excellent chemical inertness and optical transparency in water [17][26], was injected prior to the microspheres. The portion of the microfluidic channel filled with the microspheres was 15 mm long. After the microspheres insertion, home-made male connectors that minimize dead-volumes were glued to the device ports. The inlet was connected by a silicone tube with diameter 0.5 mm to a six-way injection valve (VICI Valco Instruments, USA) mounting a sample loop of 1 mL pumped by a syringe pump (Genie Touch, Kent Scientific Corporation, USA). The microfluidic device was proven to resist up to 0.8 bar of pressure during experimental conditions, without leaking.

2.3 Optical setup and measurement

A custom optical apparatus was designed and built using opto-mechanical components purchased from Thorlabs (USA) (Figure 2). A red light emitting diode (LED) with peak wavelength 625 nm was used to illuminate a slit optically conjugated to the column plane. The collimation of the beam was controlled by an iris placed at focal distance from two converging lenses. The column was imaged on a charge-coupled device (CCD) camera (Stingray, Allied Technology, Germany) by a pair of lenses that collected the back-scattered light at the angle θ_s = 135° relative to the direction of transmitted light. The microfluidic device and optical system were placed in a black enclosure to prevent spurious signals from ambient light. The intensity scattered by the packed column was measured upon flow of deionized water, NaCl water solution, water-ethanol mixtures, water solution of surfactants SDS and benzyldimethylstearylammonium chloride monohydrate (SBSAC), both purchased from Sigma-Aldrich (USA). The images captured by the CCD camera were recorded using a custom LabView program and analyzed using a custom Matlab program. The averaged intensity acquired from a selected region of the

packed column was computed as a function of time. Details on the measurement procedure, optical setup and data analysis are provided as ESM, section S2-S4.
The signal S corresponding to the relative increase of scattered light intensity I was computed as:

$$S = \frac{(I - I_0)}{(I_0 - I_f)} \quad (1)$$

where I_0 is the initial intensity measured from microspheres and I_f is the background intensity. The value of I_f was extrapolated from the dependence of I_0 on the solution refractive index n_s, measured for different concentrations of NaCl and assuming $I_0 = I_f$ for $n_s = n_b$, where $n_b = 1.331$ is the refractive index of the microspheres. The surface coverage of the micro-spheres in the packed column was estimated through the optical scattering model described in [21], which associates the measured increment of scattered intensity S to the thickness h and refractive index n_h of the adsorbed layer by:

$$S = \left(\frac{h}{h^*}\right)^2 \quad (2)$$

where $h^* = k^{-1}|n_b^2 - n_s^2|/|n_h^2 - n_s^2|$, in which k is the scattering vector defined as $k = 4\pi n_s \sin(\theta_s/2)/\lambda$.

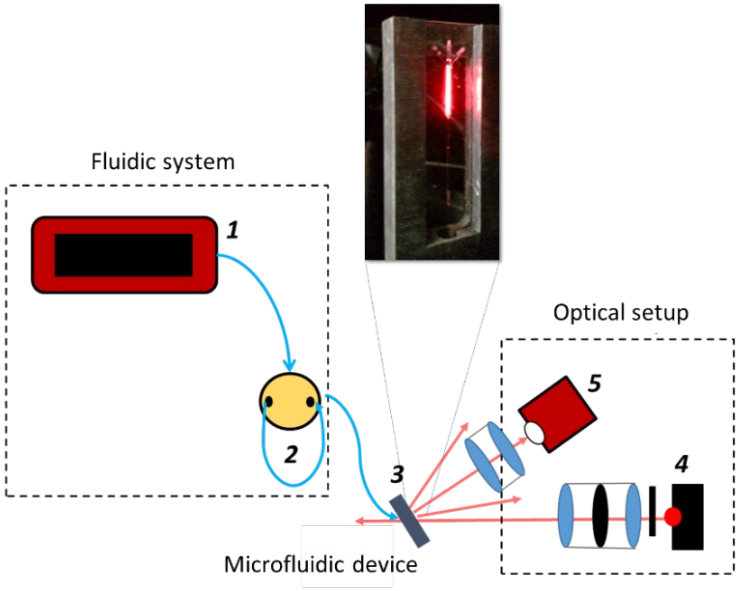

Figure 2. Schematics of the fluidic and the optical system. The fluidic system is composed by a syringe pump (1) and a six-way injection valve (2), connected to the microfluidic device (3). The channel hosting the packed column of microspheres is illuminated by the light of LED (4) and the scattered light is collected by a CCD camera (5).

3. Results and Discussion

3.1. Microfluidic device assembly

We designed and fabricated a microfluidic column made of packed WIM microspheres made of fluoropolymers providing an extraordinary low refractive index. Thanks to this property, the column is largely transparent when filled with water and becomes opaque when a molecular layer adsorbs on the surface of the microspheres, hence acting as an optical sensor based on the SPI approach. The WIM packed microspheres column was assembled by injecting the perfluorinated microspheres into the microfluidic channel (Figure 1). ~~The design of the microfluidic device ensured no optical interference and clogging~~ The size and spherical morphology of the microspheres were assessed by optical microscopy, showing a distribution of diameters of 16 ± 4 μm (Figure 1a). Considering the volume of the filled portion of the microfluidic channel (see ESM), the column contained about 10^6 microspheres. A schematic representation of the microfluidic design is shown in Figure 1c and 1d. The microspheres were introduced into the device through the central inlet using a syringe. The two side inlets were used to remove excess

material and trapped air bubbles and were closed after filling. Before each measurement, the column was washed with 30 % (v/v)ethanol for 1 h and then filled with deionized water.
The packed column was highly transparent, when filled with water (Figure 1e and 1f), due to the low refractive index of the microspheres, while it becomes opaque when a flowing solution such as ethanol or salty water (Figure 1g) passed through the column. This effectwas due to the refractive index mismatch between the volume occupied by the microspheres and that filled by the solution. However, the intensity of light scattered by the column also increased when kept in index-matching condition with water if molecules adsorbed on the microspheres surface, forming a nanometer-scale layer with different refractive index following the SPI principle. The surface density of adsorbed molecules can be quantified from the increase of scattered light intensity though a suitable optical model [21][27].

3.2. Scattered light intensity increase upon surfactant adsorption on packed microspheres

The opacity of the packed column was measured by a custom imaging setup, schematically described in Figure 2. The light of a red LED was collimated and shaped in order to illuminate only the channel hosting the packed microspheres. The column was imaged by a CCD camera and the local changes of opacity, as a function of time, were extracted by image analysis. An increase of the brightness of the image pixels was associated to an increase of the intensity of light scattered by the corresponding portion of the column. The injection of a sample containing surfactant provided a gradual increase of the opacity of the packed column up to an asymptotic steady state. The subsequent flow of pure water, after the sample solution, induced a decrease of opacity down to about the initial values. From repeated experiments on different microfluidic devices, the signal was recovered after washing within 11 % of its initial value.
We studied the optical response of the forefront region of the column upon injection of two different compounds at the concentration c_a = 30 μM: the cationic surfactant SBSAC and the anionic surfactant SDS. Figure 3 reports the measured adsorption and desorption curves. The asymptotic value of the relative increase of scattered intensity S computed through Equation 1 was about one order of magnitude larger for the cationic compound relative to the anionic surfactant (see Figure 3 caption). The characteristic time for adsorption and desorption were also very different between the two surfactants, being the absorption kinetic faster and desorption slower for the cationic compound.
The surface coverage of the microspheres in the packed column was estimated from the relative increase of scattered light intensity through Equation 2. Considering a refractive index n_h = 1.435 for SBSAC and a molecular length estimated from the chemical structure of 2.4 nm, a compact monolayer of surfactants adsorbed on the microspheres surface corresponds to a scattered intensity increase of about a factor of 10. Therefore, the measured value of S for SBSAC (Figure 3a) corresponds to 50 % of the maximum theoretical surface density of surfactant. In contrast, the smaller measured value of S for SDS (Figure 3b), for which n_h = 1.461 and the molecular length is about 1.77 nm, corresponds to only 5 % of the full coverage. In agreement with previous studies, the difference between the behaviour of the two surfactants is ascribed to a lower adsorption strength and a smaller surface density of adsorption sites for the anionic compounds on the surface of perfluorinated materials [21]. This analysis also enables to estimate the sensitivity of detection in terms of fraction of a monolayer or surfactant. Considering the background noise, the minimum detectable value of S at 3σ is 0.034, which for SBSAC corresponds to an effective thickness h = 0.14 nm and to 6 % of a compact monolayer. This value can be decreased to 1 % through time averaging over 0.5 min or less without affecting the precision of kinetic characterization, hence leading to a limit of detection (LOD) of about 1 μM for SBSAC.
These results indicate a larger adsorption strength for the cationic surfactant SBSAC than for the anionic SDS on the surface of the perfluorinated microspheres. This is in agreement with previous studies, which showed a much lower adsorption affinity and density of adsorption sites of SDS relative to SBSAC on another type of perfluorinated material, Hyflon AD® [21]. Although the proposed method relied on non-specific adsorption, a type of selectivity is provided by the different signal amplitude and kinetics observed for cationic and anionic surfactants, as shown in Figure 3. Indeed, the reduced affinity for anionic compounds is ascribed to a general property of fluorinated materials in water: their intrinsic hydrophobicity induces an accumulation of negative charges at the interface with water [28]. In agreement with the study reported in [21], the anionic surfactant also displayed a faster rate for desorption. The data reported in Figure 3c and 3d showed that the scattering signal S reached a steady state level much faster for SDS than SBSAC during the washing phase. Remarkably, the rate

corresponding to the fast relaxation component of the data in Figure 3c was $1 / \tau_{off} = 6.2 \cdot 10^{-4}$ s^{-1} , which was very similar to the value of $k_{off} = 7 \cdot 10^{-4}$ s^{-1} measured for SBSAC in [21], despite the different composition of the perfluorinated materials.

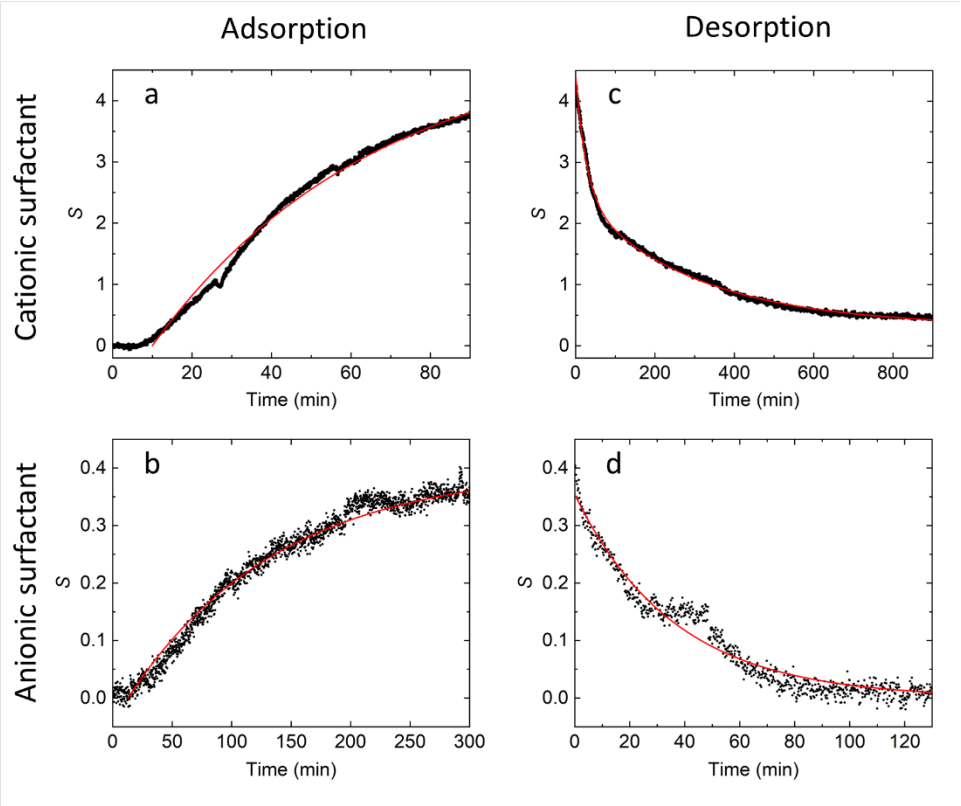

Figure 3. Optical signal from adsorption and desorption of surfactants. Relative increase S of scattered light intensity (black dots) upon injection of surfactant SBSAC (a) and SDS (b) at 30 μM and upon subsequent washing with water (c and d, respectively). The red curves are fitted to single exponential growth or decay functions with amplitude a and time constant τ: $a = 5$ and $\tau = 56$ min (a), $a = 0.4$ and $\tau = 126$ min (b), $a = 0.35$ and $\tau = 36$ min (d). The red curve in (c) is a double exponential fit with amplitudes $a_1 = 1.98$ and $a_2 = 2.12$ and time constant $\tau_1 = 27$ min and $\tau_2 = 301$ min, respectively. In (a) and (b) the fit started at 10 min and 13 min, respectively. Refractive indices of surfactant solutions and water used for washing were1.333 ±0.001.

3.3. Surfactants delay flow along the column

The proposed packed column design enabled to inspect the adsorption process in real time, along the flow direction, simply measuring the opacity of the column in different subsequent regions of the channel. We observed that the adsorption slowed the flow of surfactants through the packed column relative to the solvent (Figure 4). Figure 4a shows that a sample composed by a water-ethanol mixture provided an increase of opacity due to a change in the refractive index, with a small delay along the column gave by the flow velocity. For a flow rate of 20 μL min^{-1}, considering a bed voidance of about 0.5 [12], the flow velocity through the packed column was found to be about $v_0 = 2$ mm s^{-1} and the minimum theoretical delay across a channel length of 12 mm was about 6 s. The observed delay of about 40 s was consistent with this estimate, although it indicated a non-uniform distribution of channel size and streamlines inside the columns. In contrast, if the sample maintained a refractive index similar to that of the washing buffer, but contains molecules that bind to the surface of the microspheres, the scattering signal showed a pronounced delay along the column axis. This effect is clearly shown in Figures 4b-4d, which report the local brightness measured at different adjacent regions along the column as a function of time, after injecting 300 μM, 100 μM and 30 μM SBSAC, respectively. Decreasing the surfactant concentration c_a, we observed both, a marked decrease of the growth rate of the optical signal at the column forefront (pink curves) and an increase of the time required to propagate the signal along the column in the direction of the flow.

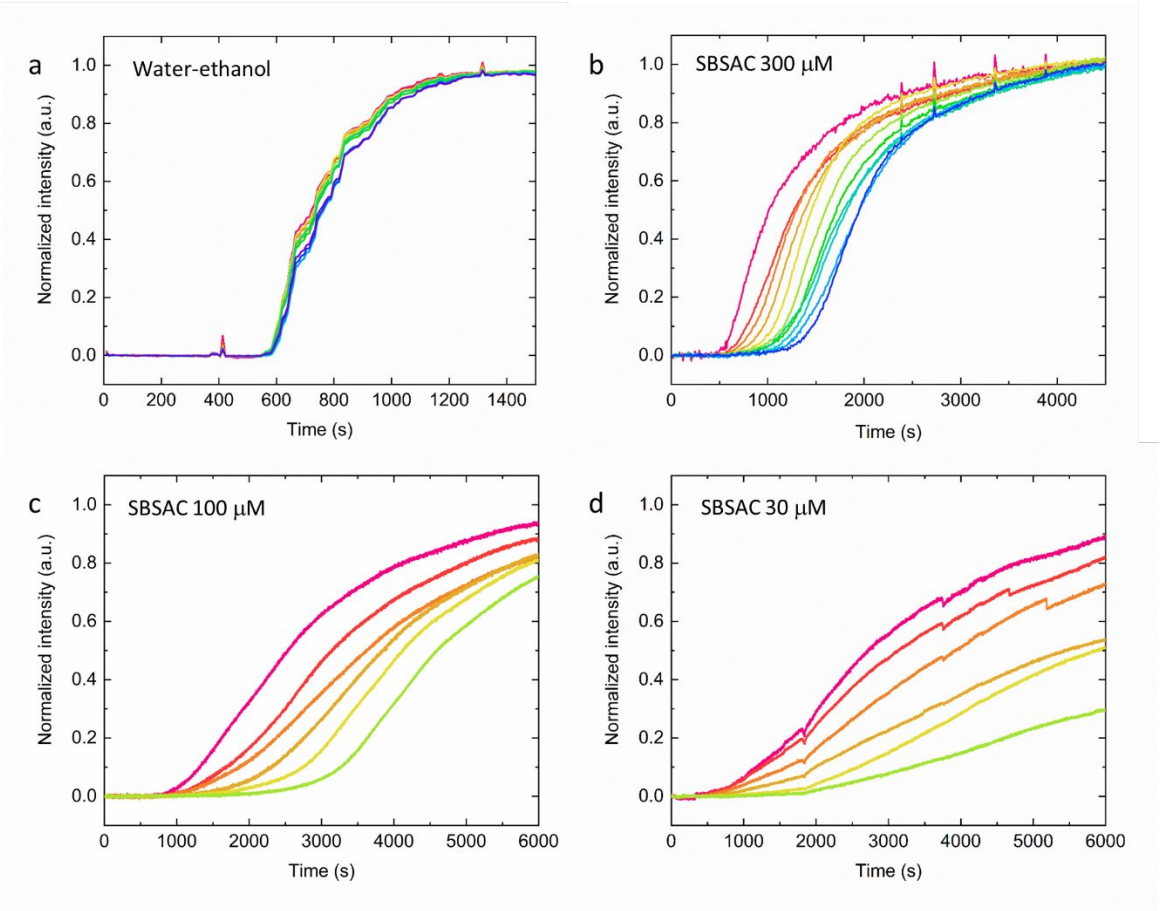

Figure 4. Optical signal measured at different positions along the column. Normalized scattered intensity as a function of time measured during the flow of (a) 50 % (v/v) water-ethanol mixture, (b) 300 µM SBSAC, (c) 100 µM SBSAC, and (d) 30 µM SBSAC. In each panel, curves represent the optical signal measured in adjacent regions of 1 mm (panels a, b, and c) or 0.8 mm (panel d) length along the packed column. The pink curves correspond to about 1 mm from the forefront and the others correspond to consecutive regions according to the same color sequence for all the panels. The value of n_s for water-ethanol (a) is 1.360 ±0.001, whereas of n_s = 1.360 ±0.001 for surfactant solutions (b, c and d).

~~The matching of microspheres and solution refractive index enables to monitor the velocity of the surfactant inside the packed column.~~ ~~The delay of the opacity increases from the inlet to the outlet of the column whereas the shape of the adsorption curves remains similar.~~ The access to the measurement of surfactant adhesion on the microspheres and propagation velocity inside the column was granted by the WIM conditions. The delay time of the initial growth of the adsorption curves was related to the velocity of surfactants through the streamlines, when the surface of the microspheres was not saturated by the adsorbate yet. Figure 5a reports the delay time as a function of the position along the column and showed a linear dependence for all cases reported in Figure 4, hence indicating constant velocities along the column. For 300 µM SBSAC, we obtained a velocity v_a = 11.9 µm s^{-1}, which is much smaller than the velocity v_0 = 290 µm s^{-1} of the pure solvent ~~indicated by the delay time~~ obtained from the data of Figure 4a. Even smaller propagation velocities,2.6 µm s^{-1} and 1.1 µm s^{-1}, where measured for 100 mM and 300 mM SBSAC, respectively. ~~This strong reduction of the velocity of surfactant is ascribed to the reversible adsorption of the molecules on the microspheres.~~ The signal propagation velocity v_a displayed a linear dependence on surfactant concentration, as reported in Figure 5b.

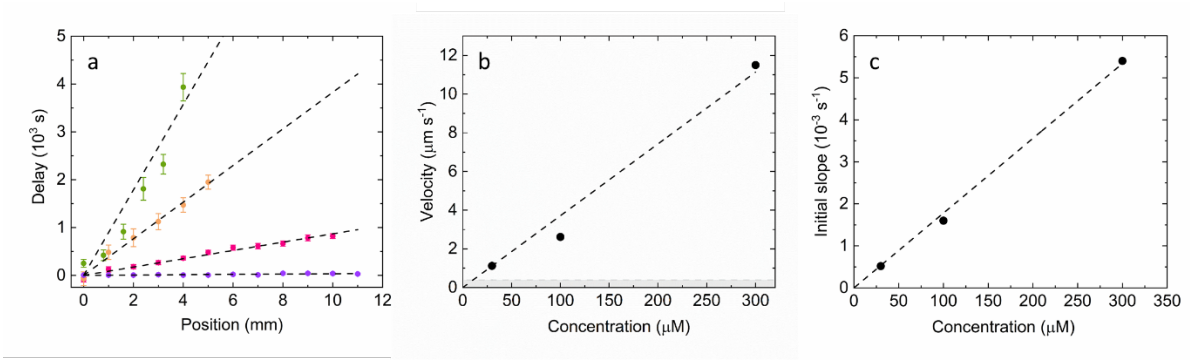

Figure 5. Dependence of optical signal response on SBSAC concentration. (a) Delay of the optical signal along the packed column obtained from the curves of Figure 4. Delay time corresponding to 30 % of the asymptotic amplitude of the intensity curves are reported for 30 μM SBSAC (green), 100 μM SBSAC (orange), 300 μM SBSAC (red), and 50 % (v/v) water-ethanol (violet). Error bars correspond to the effect of intensity noise on the delay time measurement. The dashed lines are linear fits to the data points. (b) Velocities of the optical signal increase along the column obtained from the linear fits of panel a. The dashed line is a linear fit and the grey area represents the uncertainty on the velocity measurement at low SBSAC concentrations. (c) Average speed of growth of the optical signal at 30 % of the maximum amplitude obtained from the SBSAC data of Figure 4.

In general, the velocity v_a observed in presence of adsorption was related to the velocity v_0 through the retention ratio R, as $v_a = Rv_0$. The dependence of R on the surfactant concentration indicated the amount of molecules retained in a unit volume of the column. Since $R << 1$, the surfactant reached the terminal part of the column when the forefront region approached saturation. The flux of molecules along the column was reduced by a factor, corresponding to the quantity of molecules subtracted from the mobile phase per unit volume by adsorption or not contributing to the signal because of channelling. In case of an ideal packing, $R \approx c_a / c^*$, where c^* is the concentration of binding sites in the column. The slope reported in Figure 5b corresponded to $c^* = 8$ mM, a value much larger than the expected concentration of adsorption sites in the column, 0.4 mM, which was estimated considering an adsorption area per SBSAC molecule of 0.73 nm^2 [21]. This suggested the presence of void regions in the column, yielding to loss of sample through channelling. The detection performance of the method was expected to get largely improved in case of having an ideal packing of the microspheres.

The delay of the signal-increase along the column represented an analytical parameter that can be converted to concentration values of an unknown sample, through the calibration plot reported in Figure 5b. However, in the current configuration, the precision on the determination of the delay at low concentrations (grey region in Figure 5b) limited the detection to values of 10 μM for the investigated cationic surfactant. A more sensitive analytical parameter was given by the rate of growth of the optical signal at the forefront region of the column, which corresponded to the maximum slope of the pink curves in Figures 4b-4d. Figure 5c shows that the signal-growth rate linearly scaled with the value of the concentration, c_s. By averaging the signal over 30 s and for an observation time of about 1 h, the LOD at 3σ of the baseline noise corresponded to about 1 μM of SBSAC (440 ng mL^{-1}), which was in agreement with the same value reported above, estimated from the amplitude of the signal at saturation. Several methods were proposed to quantify cationic surfactants in water, as summarized in ESM (Table S1), with LODs spread over a large range, 3 ng mL^{-1} [29] - 4 μg mL^{-1} [30]. The method proposed in this work combines a LOD within this range with a microfluidic design and regeneration capability that makes it suitable for online water monitoring platforms.

5. Conclusions

In this work, we demonstrated a novel class of microfluidic chromatography device based on WIM micro-spheres offering the advantage of real time and label-free visualization of binding profiles inside the packed column without fluorescence markers. We showed that cationic and anionic surfactants provided different kinetic sensorgrams ascribed to their adsorption strength on the perfluorinated microspheres and kinetics. The proposed system provided access to a novel analytical parameter, time evolution of the binding profile within the column, through label-free visualisation. The system can be regenerated by washing and is based on a simple optical detection system, which makes it suitable for its integration into compact analytical platforms. The current

detection performance is mainly limited by the non-uniform packing of the microspheres. The proposed microfluidic design facilitates the insertion of the microspheres and the removal of air bubbles, which is a major problem in microfluidic packed microcolumns. Therefore, further developments are required to increase the uniformity of the packing and to make the device fabrication protocol suitable for industrial scale production. The selectivity ascribed to adsorption is low, although is enough to discriminate between cationic and anionic surfactants. An increased selectivity can be in principle achieved by including a functionalization step of the microsphere surfaces with specific molecular probes.

References

1. Ivanković T, Hrenović J (2010) Surfactants in the Environment. Arch Ind Hyg Toxicol 61:95–110. https://doi.org/10.2478/10004-1254-61-2010-1943
2. Hernández F, Ibáñez M, Portolés T, et al (2015) Advancing towards universal screening for organic pollutants in waters. J Hazard Mater 282:86–95. https://doi.org/10.1016/j.jhazmat.2014.08.006
3. Kutter JP (2012) Liquid phase chromatography on microchips. J Chromatogr A 1221:72–82. https://doi.org/10.1016/j.chroma.2011.10.044
4. Ahmad AL, Low SC, Shukor SRA, et al (2010) Hindered diffusion in lateral flow nitrocellulose membrane: Experimental and modeling studies. J Memb Sci 357:178–184. https://doi.org/10.1016/j.memsci.2010.04.018
5. Malmstadt N, Yager P, Hoffman AS, Stayton PS (2003) A Smart Microfluidic Affinity Chromatography Matrix Composed of Poly(N -isopropylacrylamide)-Coated Beads. Anal Chem 75:2943–2949. https://doi.org/10.1021/ac034274r
6. Jemere AB, Martinez D, Finot M, Harrison DJ (2009) Capillary electrochromatography with packed bead beds in microfluidic devices. Electrophoresis 30:4237–4244. https://doi.org/10.1002/elps.200900334
7. Flemming JH, Baca HK, Werner-Washburne M, et al (2006) A packed microcolumn approach to a cell-based biosensor. Sensors Actuators B Chem 113:376–381. https://doi.org/10.1016/j.snb.2005.03.098
8. Kralj JG, Arya C, Tona A, et al (2012) A simple packed bed device for antibody labelled rare cell capture from whole blood. Lab Chip 12:4972. https://doi.org/10.1039/c2lc41048f
9. Sadavarte R, Madadkar P, Filipe CD, Ghosh R (2018) Rapid preparative separation of monoclonal antibody charge variants using laterally-fed membrane chromatography. J Chromatogr B 1073:27–33. https://doi.org/10.1016/j.jchromb.2017.12.003
10. Ng JK-K, Feng H, Liu W-T (2007) Rapid discrimination of single-nucleotide mismatches using a microfluidic device with monolayered beads. Anal Chim Acta 582:295–303. https://doi.org/10.1016/j.aca.2006.09.016
11. Kim J, Heo J, Crooks RM (2006) Hybridization of DNA to Bead-Immobilized Probes Confined within a Microfluidic Channel. Langmuir 22:10130–10134. https://doi.org/10.1021/la0616956
12. Shapiro MS, Haswell SJ, Lye GJ, Bracewell DG (2009) Design and characterization of a microfluidic packed bed system for protein breakthrough and dynamic binding capacity determination. Biotechnol Prog 25:277–285. https://doi.org/10.1002/btpr.99
13. Cacheux J, Brut M, Bancaud A, et al (2018) Spatial Analysis of Nanofluidic-Embedded Biosensors for Wash-Free Single-Nucleotide Difference Discrimination. ACS Sensors 3:606–611. https://doi.org/10.1021/acssensors.7b00667
14. Zanchetta G, Lanfranco R, Giavazzi F, et al (2017) Emerging applications of label-free optical biosensorsz. Nanophotonics 6:. https://doi.org/10.1515/nanoph-2016-0158
15. Giavazzi F, Salina M, Cerbino R, et al (2013) Multispot, label-free biodetection at a phantom plastic–water interface. Proc Natl Acad Sci 110:9350–9355. https://doi.org/10.1073/pnas.1214589110
16. Giavazzi F, Salina M, Ceccarello E, et al (2014) A fast and simple label-free immunoassay based on a smartphone. Biosens Bioelectron 58:395–402. https://doi.org/10.1016/j.bios.2014.02.077
17. Lanfranco R, Buscaglia M (2016) Invisible Fluorinated Materials for Optical Sensing. In: Reference Module in Materials Science and Materials Engineering. Elsevier
18. Salina M, Giavazzi F, Ceccarello E, et al (2016) Multi-spot, label-free detection of viral infection in complex media by a non-reflecting surface. Sensors Actuators B Chem 223:957–962. https://doi.org/10.1016/j.snb.2015.09.122
19. Zilio C, Bernardi A, Palmioli A, et al (2015) New “clickable” polymeric coating for glycan microarrays. Sensors Actuators, B Chem 215:. https://doi.org/10.1016/j.snb.2015.03.079
20. Nava G, Ceccarello E, Giavazzi F, et al (2016) Label-free detection of DNA single-base mismatches using a simple reflectance-based optical technique. Phys Chem Chem Phys 18:13395–13402. https://doi.org/10.1039/C5CP08017G

21. Lanfranco R, Giavazzi F, Salina M, et al (2016) Selective Adsorption on Fluorinated Plastic Enables the Optical Detection of Molecular Pollutants in Water. Phys Rev Appl 5:054012. https://doi.org/10.1103/PhysRevApplied.5.054012
22. Lanfranco R, Giavazzi F, Bellini T, et al (2020) Fabrication and Optical Modeling of Micro-Porous Membranes Index-Matched with Water for On-Line Sensing Applications. Macromol Mater Eng 305:1900701. https://doi.org/10.1002/mame.201900701
23. van de Hulst HC (1957) Light Scattering by Small Particles. Dover, New York
24. Saez J, Etxebarria J, Antoñana-Diez M, Benito-Lopez F (2016) On-demand generation and removal of alginate biocompatible microvalves for flow control in microfluidics. Sensors Actuators B Chem 234:1–7. https://doi.org/10.1016/j.snb.2016.04.140
25. Saez J, Antonana M, Etxebarria J, Benito-Lopez F (2015) In-situ generated biocompatible alginate actuators for flow control in microfluidics. In: 2015 Transducers - 2015 18th International Conference on Solid-State Sensors, Actuators and Microsystems (TRANSDUCERS). IEEE, pp 2132–2135
26. Merkel TC, Pinnau I, Prabhakar R, Freeman BD (2006) Gas and Vapor Transport Properties of Perfluoropolymers. In: Materials Science of Membranes for Gas and Vapor Separation. John Wiley & Sons, Ltd, Chichester, UK, pp 251–270
27. Lanfranco R, Saez J, Di Nicolò E, et al (2018) Phantom membrane microfluidic cross-flow filtration device for the direct optical detection of water pollutants. Sensors Actuators B Chem 257:924–930. https://doi.org/10.1016/j.snb.2017.11.024
28. Kudin KN, Car R (2008) Why Are Water−Hydrophobic Interfaces Charged? J Am Chem Soc 130:3915–3919. https://doi.org/10.1021/ja077205t
29. Shrivas K, Sahu S, Ghorai A, Shankar R (2016) Gold nanoparticles-based colorimetric determination of cationic surfactants in environmental water samples via both electrostatic and hydrophobic interactions. Microchim Acta 183:827–836. https://doi.org/10.1007/s00604-015-1689-z
30. Öztekin N, Erim FB (2005) Determination of cationic surfactants as the preservatives in an oral solution and a cosmetic product by capillary electrophoresis. J Pharm Biomed Anal 37:1121–1124. https://doi.org/10.1016/j.jpba.2004.07.050